Rheol Acta (2004) 44: 1–15
DOI 10.1007/s00397-004-0398-z

ORIGINAL CONTRIBUTION

**Martin Sentmanat**
**Edward B. Muliawan**
**Savvas G. Hatzikiriakos**

# Fingerprinting the processing behavior of polyethylenes from transient extensional flow and peel experiments in the melt state

Received: 22 March 2004
Accepted: 4 May 2004
Published online: 16 July 2004


M. Sentmanat
Senkhar Technologies, LLC,
Akron, Ohio, USA

E. B. Muliawan · S. G. Hatzikiriakos (✉)
Department of Chemical and Biological Engineering, The University of British Columbia, Vancouver,
British Columbia, Canada
E-mail: hatzikir@interchange.ubc.ca

**Abstract** The flow curves of linear (linear-low and high density) and branched polyethylenes are known to differ significantly. At increasing shear rates, the linear polymers exhibit a surface melt fracture or sharkskin region that is followed by an unstable oscillating or stick-slip flow regime when a constant piston speed capillary rheometer is used. At even higher shear rates, gross melt fracture appears. Unlike their linear counterparts, branched polyethylenes rarely exhibit sharkskin melt fracture and although gross melt fracture appears at high shear rates there is no discontinuity in their flow curve. The various flow regimes of these two types of polyethylenes are examined by performing experiments in the melt state using a unique extensional rheometer (the SER by Xpansion Instruments) that is capable of performing accurate extensional flow and peel experiments at very high rates not previously realized. The peel strength curves of these linear and branched polyethylenes exhibit all of the distinct flow regimes exhibited in their respective flow curves, thereby providing a fingerprint of their melt flow behavior. Moreover, these extensional flow and peel results in the melt state provide insight into the origins and mechanisms by which these melt flow phenomena may occur with regard to rapid tensile stress growth, melt rupture, and adhesive failure at the polymer wall interface.

**Keywords** Extensional flow · Sharkskin · Stick-slip · Gross melt fracture · Polyethylenes · Peel · Processing behavior

## Introduction

Molten linear polyethylenes in capillary flow exhibit many idiosyncrasies such as wall slip and melt fracture phenomena (Bagley et al.1958; Lupton and Regester1965; Myerholtz1967; Blyler and Hart1970; Ramamurthy1986; Hatzikiriakos and Dealy 1992a, 1992b). A typical flow curve of such a polymer consists of two distinct branches, a no-slip (or weak slip)/low-flow branch (also known as sharkskin melt fracture flow regime due to small amplitude periodic distortions that appear on the extrudate surface), and a slip/high-flow branch (also known as gross melt fracture flow regime due to gross distortions that appear on the extrudate surface). These two distinct branches are separated by a certain range of apparent shear rates over which the flow ceases to be stable first observed by Bagley et al. (1958). In a constant-rate piston-driven capillary rheometer, the pressure oscillates between two extreme values independent of the apparent shear rate. This phenomenon is known as oscillating, cyclic or stick-slip melt fracture. On the other hand, in a constant-pressure capillary rheometer, the flow rate oscillates between two extreme values, a phenomenon known as spurt.

Contrary to this variability of phenomena for linear polyethylenes (sharkskin, oscillating and gross melt fracture), only gross melt fracture has been reported for branched polyethylenes (Ramamurthy1986). This certainly has to do with slip at the wall that might occur easier in the case of linear polyethylenes, i.e., a sudden change from a weak to a strong slip at a critical shear stress value.

In the sharkskin flow regime of linear polyethylenes several investigators have reported the occurrence of wall slip (Smoluk1964; Blyler and Hart1970; Ramamurthy1986; Kalika and Denn1987; Hatzikiriakos and Dealy 1992a). The mechanism by which this weak slip takes place has also been investigated. For example, it is interesting to know whether or not wall slip is due to failure at the polymer-wall interface (adhesive failure) or to failure within the polymer but very close to the wall (cohesive failure). Hill et al. (1990) have developed an adhesive slip velocity model that was found to be consistent with slip experimental measurements reported by Kalika and Denn (1987). Similarly, Hatzikiriakos (1993), assuming adhesive failure of the polymer-wall interface as a requirement for the occurrence of slip, has developed a slip velocity model that was found to be consistent with experimental measurements. Anastasiadis and Hatzikiriakos (1998) have provided additional evidence that the onset of the weak slip might indeed be adhesive in nature. On the other hand, many reports claim that sharkskin of polyethylenes has not been found to be accompanied by wall slip and that the polymer melt under these conditions sticks to the wall (El-Kissi and Piau1994; Wang et al.1996; Legrand and Piau1998; Inn et al.2000; Migler et al.2001). Therefore, there is no general agreement on whether or not a weak slip is true in the case of molten polymers exhibiting sharkskin.

The mechanism of sharkskin has also long been debated in the literature. The two most popular ideas are the *exit stick-slip* (Wang et al.1996) and the rupture hypothesis (Cogswell1972; Migler et al.2001) with the latter having found wider acceptance. The hypothesis of rupture does not explicitly say anything about whether or not this is adhesive or cohesive, a question of fundamental nature.

Gross fracture is accompanied by the occurrence of strong slip at least in the case of linear polyethylenes (second high flow rate branch). Estimations of velocity profiles have lead to a conclusion that the profile is almost plug-like (Smoluk1964; Blyler and Hart1970; Ramamurthy1986; Kalika and Denn1987; Hatzikiriakos and Dealy 1992b). However, once again with regard to the mechanism of this strong slip it remains uncertain whether this slip behavior is a result of a purely adhesive failure or a cohesive one at a layer within the polymer but very close to the wall.

In this paper, we report on the melt fracture of several linear (LLDPE) and branched (LDPE) polyethylenes. Transient extensional flow and dynamic peel results for these polymers at elevated temperatures are also reported. As will be seen, the peeling experiments provide a fingerprint of extrusion behavior, tracking essentially all flow regimes observed in capillary extrusion, i.e., discontinuity in the flow curve and flow instability. Since the interfaces or surfaces at which failure occurs can be easily observed in peeling experiments, conclusions can safely be drawn about the nature of failure in each regime. These conclusions are extended to extrusion experiments and together with the extensional melt flow characterizations new insight into the general problem of melt fracture is gained. It should be noted that peeling experiments were also performed by Hill et al. (1990) on polymers at room temperature, the results of which were used to develop an adhesive slip velocity model as discussed above. However, at temperatures below the melting point, the failure is almost always adhesive in nature as the cohesive strength of the solid polymer is high except for ultra high purity interfaces. As will be seen in this paper, when the peeling experiments are performed at molten temperatures new features emerge and the failure might be cohesive, adhesive or an unstable combination of the two (stick-slip) depending on the nature of the polymer and the peeling rate.

## Experimental

Experiments were performed on four different commercial polymers of identical microstructure but of varying macrostructure: (a) two film grade linear low-density polyethylenes—one metallocene-catalyzed (Exact 3128 from Exxon Mobil) and one ZieglerNatta polymer (LL3001.32 from Exxon Mobil), and (b) two low-density polyethylenes—a film grade (EF606 from Westlake Polymers) and a coating grade (LD200 from Exxon Mobil). These polymers were rheologically characterized in linear viscoelastic (LVE) simple shear using an ARES rotational rheometer and in simple extension using an SER Universal Testing Platform (Sentmanat 2003a, 2003b,2004; Sentmanat et al.2004) from Xpansion Instruments. As depicted in Fig. 1 and further described by Sentmanat (2004), the SER unit is a dual windup extensional rheometer that has been specifically designed for use as a detachable fixture on a variety of commercially available rotational rheometer host platforms. The particular SER model used in this study, the SER-HV-A01, was designed for use on an ARES rotation rheometer host system and in simple extension mode is capable of generating Hencky strain rates up to 20 $s^{-1}$ under controlled temperatures in excess of 250 °C.

As described by Sentmanat (2004) the SER is also capable of performing controlled rate and temperature

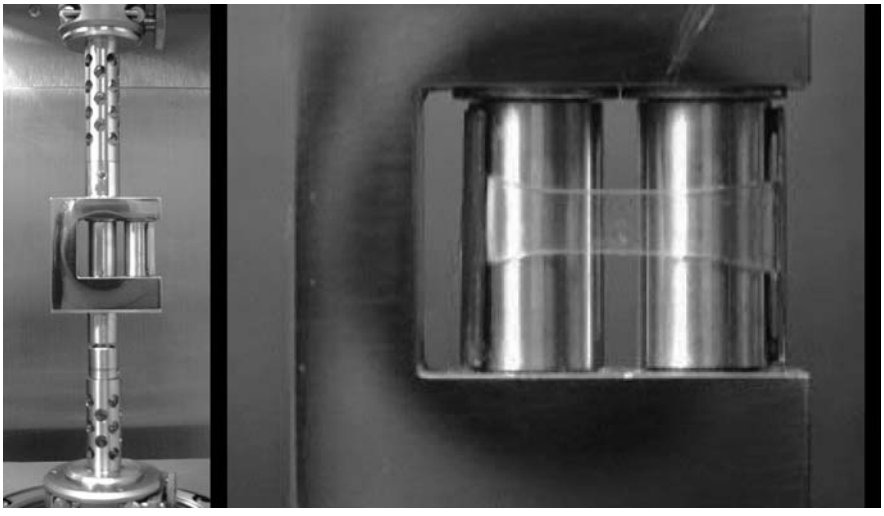

**Fig. 1** SER Universal Testing Platform shown mounted and in operation during an extensional flow experiment with a polymer melt sample

peel measurements and was used in this study to determine the dynamic peeling behavior of all four polyethylenes at a melt temperature of 150 °C. Peel specimens were prepared by first compression molding polymer samples to a fixed gage thickness between two sheets of white copier paper, then using a dual blade cutter, fixed width peel specimens were prepared and attached to the securing clamps of the SER drums as shown in Fig. 2. Upon loading the specimens onto the pre-heated SER fixture, the specimens were allowed to reach temperature prior to performing peel measurements at linear peel rates controlled by the circumferential speed of the SER drums.

A standard Instron piston-driven constant-speed capillary unit was used to assess the processability of this polymer in terms of critical shear rates for the onset of sharkskin, oscillating and gross melt fracture. A capillary die having a length-to-diameter ratio of L/D = 16, a diameter D = 1 mm and a contraction angle of $2\alpha = 180°$ was used. No Bagley correction was applied to the data and the results are presented in terms of apparent shear stress, defined as $\sigma_A = P_d D/4L$, where $P_d$ is the driving pressure measured at the entrance to the capillary, and apparent shear rate defined as $\dot{\gamma} = 4Q/\pi D^3$ , where Q is the volumetric flow rate.

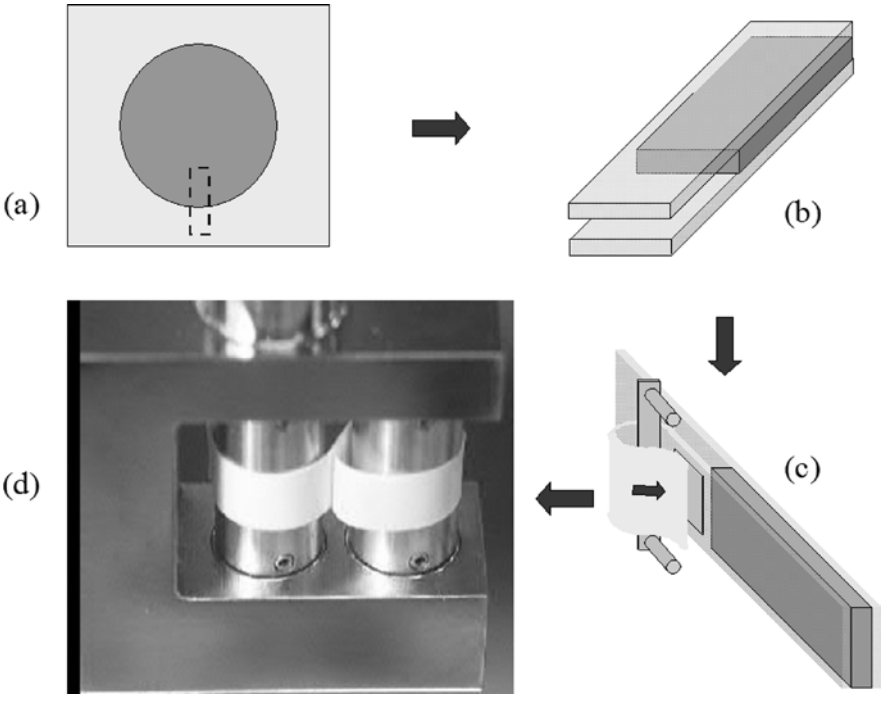


**Fig. 2a–c** Schematic illustration of cut-to-width T-peel polymer specimen preparation: **a** compression molded polymer sample between sheets of paper substrates; **b** peel specimens cut-to-width using a dual blade cutter; **c** peel specimen loaded onto sample securing clamps of the SER; **d** SER during a dynamic peel experiment

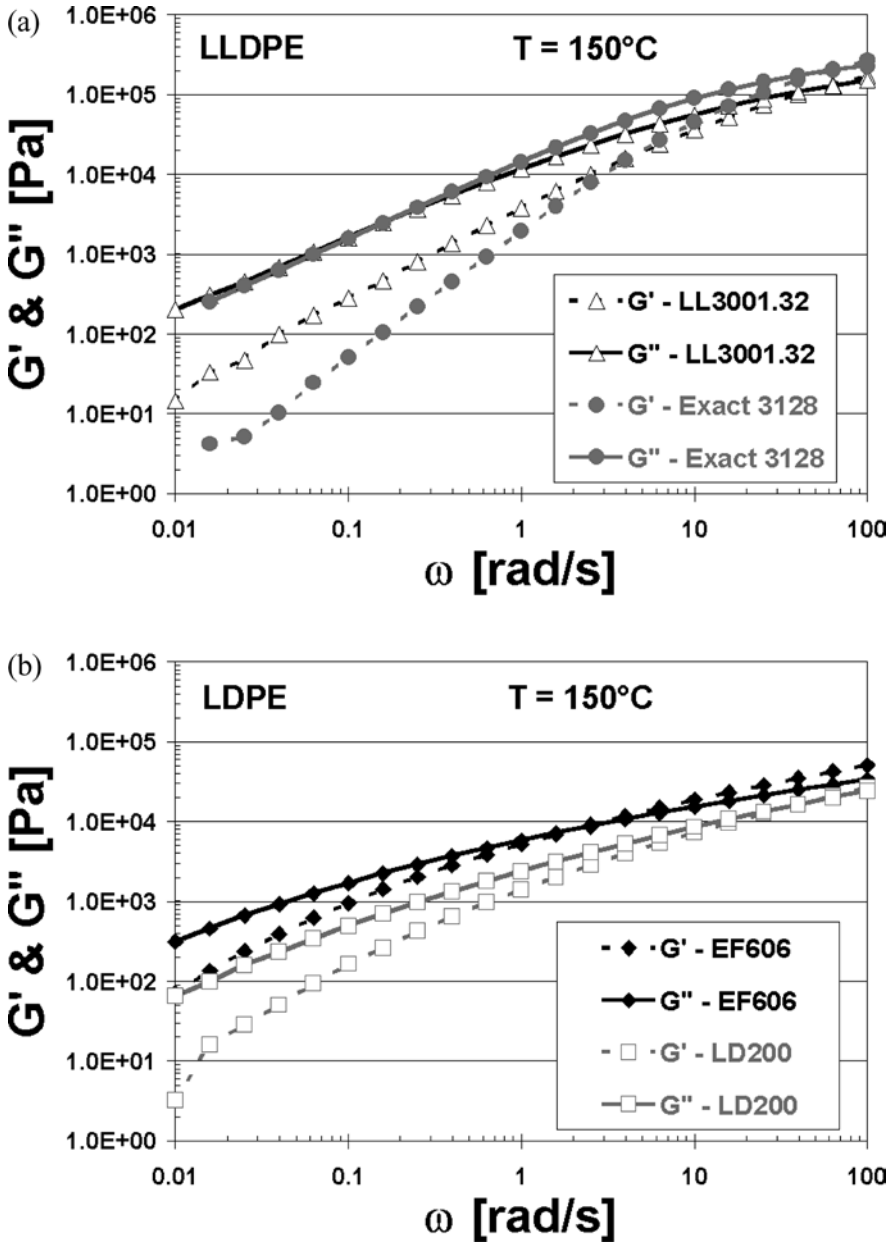


**Fig. 3a,b** The linear viscoelastic moduli at a temperature of 150 °C for: **a** the LLDPEs LL3001.32 and Exact 3128; **b** the LDPEs EF606 and LD200

## Rheological characterization

Linear viscoelasticity

Figure 3a,b contains plots of the linear viscoelastic moduli of the LLDPEs and LDPEs respectively. As reflected in Fig. 3a, despite exhibiting lower loss modulus values the Exact 3128 melt exhibits higher storage modulus values than the LL3001.32, a reflection of the narrow molecular weight distribution of Exact 3128 (PI≈2) that is common for metallocene-catalyzed polyethylenes. In the case of the LDPEs, the LD200 exhibits lower storage and loss modulus values than the EF606, a reflection of the lower molecular weight inherent with coating grade polymers.

Figure 4 contains plots of the LVE shear relaxation modulus of all four polymers at 150 °C taken from cone and plate measurements at a step shear of 10%. It can be seen that the LL3001.32 has a broader relaxation spectrum than its other linear counterpart, behavior suggesting both a higher molecular weight and a broader molecular weight distribution. Despite exhibiting much lower modulus at short relaxation times, the two LDPEs possess an even broader distribution of relaxation times than the LL3001.32, behavior consistent with highly branched polymer macrostructure. Comparing just the

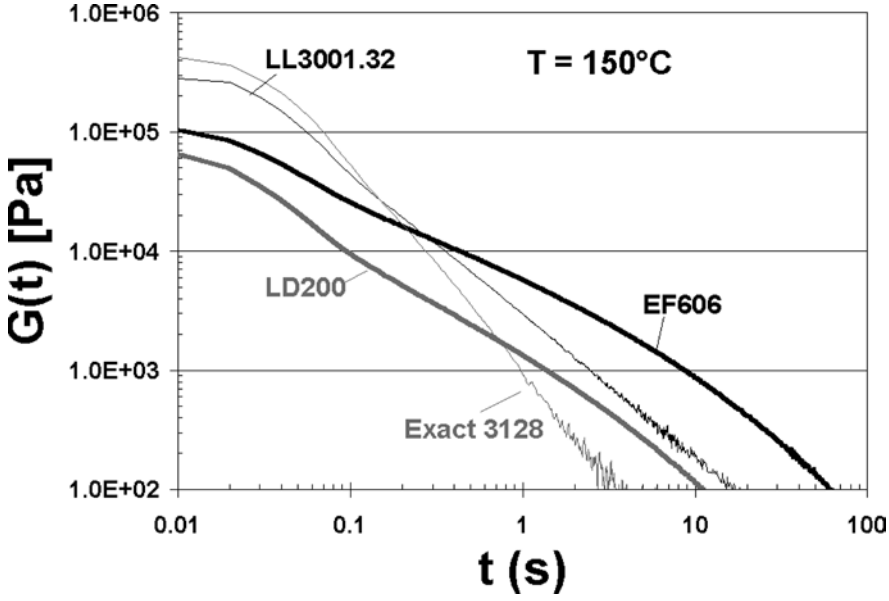


**Fig. 4** LVE relaxation modulus of all four polymers at a melt temperature of 150 °C

two LDPEs, the EF606's higher modulus again indicates a higher molecular weight than the LD200.

## Extensional rheology

Figure 5a,b contains tensile stress growth plots that provide a characterization of the extensional melt flow behavior of the LLDPEs and LDPEs respectively. Superposed with the tensile growth curves in Fig. 5a,b is the LVE shear stress growth plot of $3\eta^+$ for each polymer taken from start-up of steady simple shear experiments with cone and plate, which from theory describes the LVE envelope of tensile stress growth behavior. Comparing first the linear polymers in Fig. 5a, the agreement of the low-strain tensile portions of the tensile stress growth curves with the cone and plate data provides an experimental validation of Trouton's law. At low Hencky strain rates and long times, the tensile stress growth curves deviate little from the predicted LVE behavior and the higher plateau viscosity corresponding to $3\eta_0$ for the LL3001.32 polymer provides further evidence of a higher molecular weight. However, with increasing Hencky strain rate the tensile stress growth curves show strain hardening behavior manifested as a deviation from the predicted LVE stress growth behavior with the Exact 3128 polymer exhibiting significantly higher growth than LL3001.32 as reflected by the data at rates of 10 and 20 $s^{-1}$. Hence, despite having a slightly lower viscosity at low rates of deformation, at very high extensional rates the Exact 3128 melt exhibits significantly higher peak tensile stress and elastic flow behavior than the other linear polymer. Furthermore, with increasing Hencky strain rate, the specimen rupture transitions from a ductile mode of failure to a brittle-type mode of failure manifested by an abrupt sample fracture at rates above 1 $s^{-1}$ for the Exact 3128 and at rates above 10 $s^{-1}$ for the LL3001.32.

Comparing now the extensional flow data for the branched polymers in Fig. 5b, the low-strain portions of the tensile stress growth curves deviate little from the LVE predictions taken from the cone and plate data and as expected indicate a significantly lower melt viscosity for the coating grade LD200 polymer. However, at a characteristic Hencky strain both polymers exhibit significant strain hardening manifested by a rapid stress rise and significant deviation from LVE behavior with increasing strain. Despite having a much lower viscosity in simple shear and in the LVE regime, the LD200 polymer exhibits significantly larger strain hardening such that its peak tensile stress approaches that of the higher melt flow viscosity film grade polymer for a given rate of Hencky strain, an observation that suggests the presence of much higher molecular weight long-chain branching with the LD200.

Comparing now the extensional flow behaviors of the linear polymers with the branched polymers, with increasing rate of extension the linear polymers exhibit a much higher elastic modulus than the branched polymers as reflected in the comparative true stress vs true strain curves of Fig. 6 for a Hencky strain rate of 20 $s^{-1}$. In addition, it is evident from the data in Fig. 6 that the strain at rupture is inherently higher for the branched polymers at these high rates of extension. Hence, at very short times and high rates of extension the presence of polymer chain branching appears to have an energy retardation effect on the extensional flow behavior of polymers. In the case of long-chain branched polymers, it is believed that the energy that would normally be borne by the polymer chain backbone upon the initia-

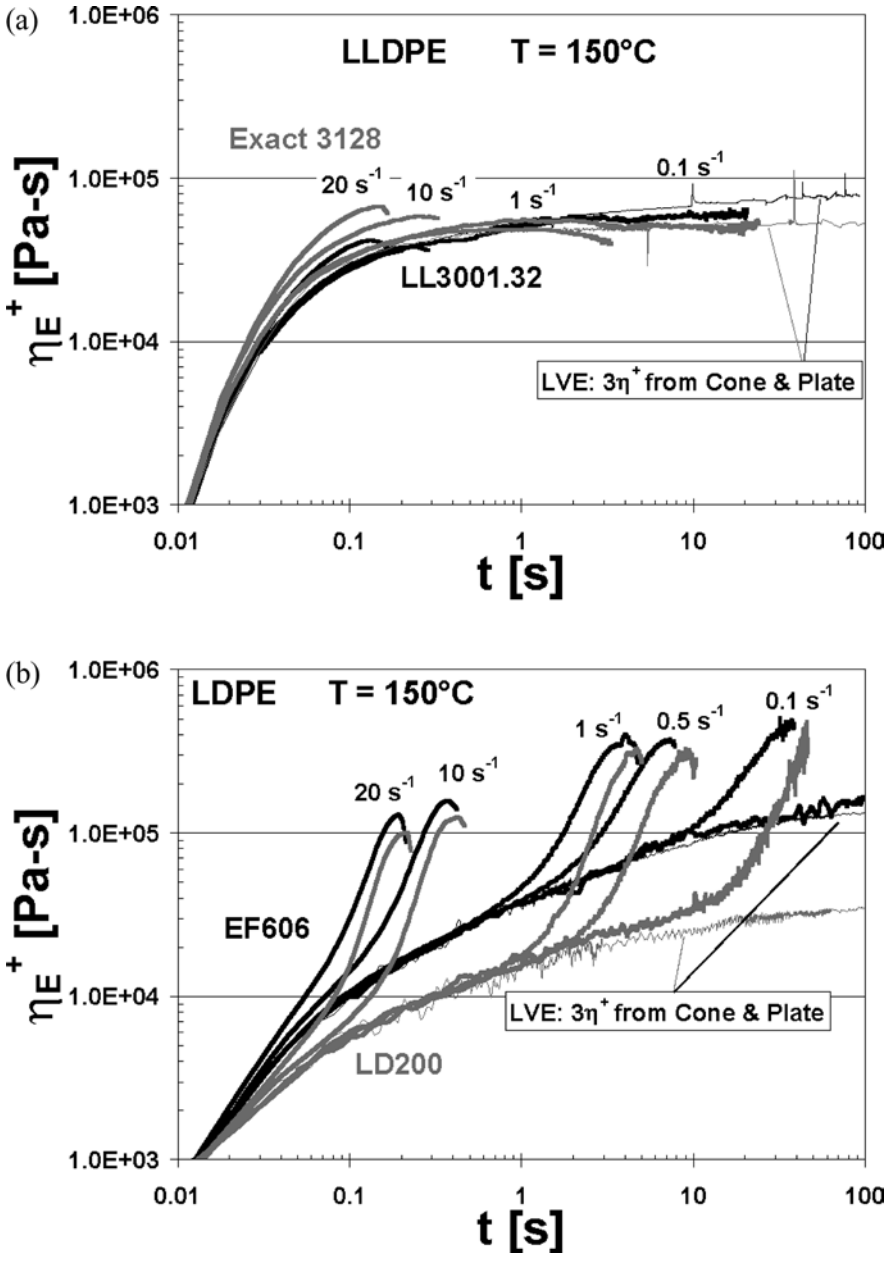


**Fig. 5a,b** The tensile stress growth curves over a range of Hencky strain rates from 0.1 to 20 $s^{-1}$ at a melt temperature of 150 °C for: **a** the LLDPEs LL3001.32 and Exact 3128; **b** the LDPEs EF606 and LD200

tion of high extensional flow rates is dissipated somewhat by the associative flow and deformation behavior of long-chain branches along the backbone. Although with increasing extensional deformation the presence of long-chain branching subsequently contributes to backbone stretch (McLeish and Larson1998), the initial tensile retardation of the elastic modulus appears to delay the propagation of melt rupture of branched polymers. As will be subsequently discussed, this tensile retardation mechanism is believed to play an important role in observed melt processing behavior, particularly with regard to sharkskin melt fracture.

## Capillary extrusion

Fig. 7a–d contains plots of the apparent flow curve for each of the polymers used in this study. From Fig. 7a,b it can be seen that the flow curves of the two LLDPEs exhibit a marked discontinuity consisting of two distinct flow curve branches separated by a range of apparent shear rates where the flow is unstable. In the low flow rate branch, sharkskin is obtained on the surface of extrudates when the shear stress exceeds a critical value, whereas in the high flow rate branch, gross melt fracture

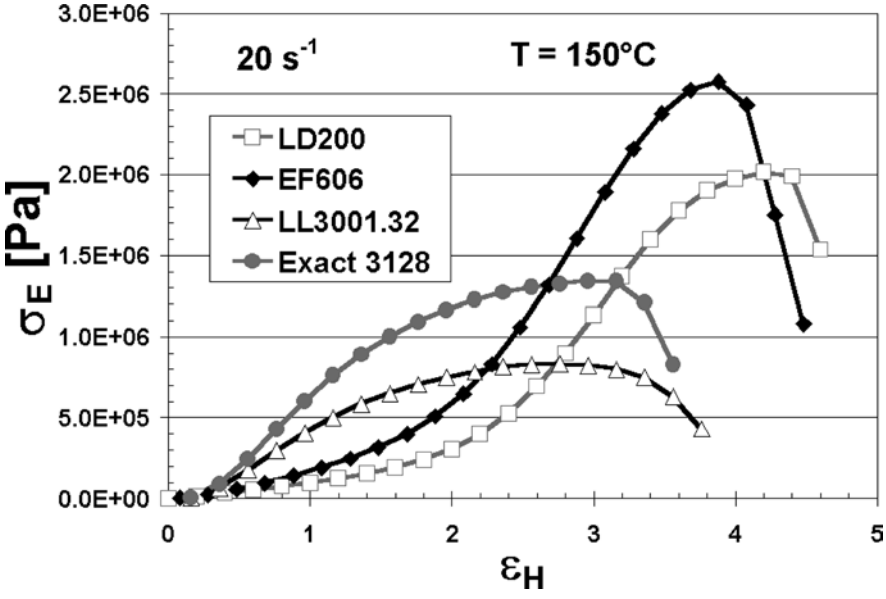


**Fig. 6** True tensile stress vs Hencky strain curves for all four polymers at a Hencky strain rate of 20 $s^{-1}$ and a melt temperature of 150 °C

eventually appears. It is worth noting that the Exact 3128 polymer, which displays a much higher elastic modulus at high rates of extension, exhibits an earlier onset to sharkskin melt fracture and a much larger flow curve discontinuity than the LL3001.32 polymer. Figure 8 depicts typical extrudate photos of LLDPE (LL3001.32) at 150 °C obtained from a capillary rheometer using a capillary having L/D = 16, D = 1 mm and a contraction angle of 180°.

Contrary to this behavior, the flow curves of the two LDPEs as depicted in Fig. 7c,d consist of a single continuous flow curve, where the extrudate is initially smooth at low rates and then becomes grossly distorted at higher rates. The transition is rather abrupt, occurring over a short range of apparent shear rates, and unlike the linear polymers, the LDPEs do not exhibit sharkskin melt fracture. Figure 9 depicts typical extrudate photos of LDPE (EF606) at 150 °C obtained from a capillary rheometer using a capillary having L/D = 16, D = 1 mm and a contraction angle of 180°.

Figures 10 and 11 depict typical experimental runs for the two LLDPEs under conditions where stick-slip is obtained. Experiments for two and four shear rates are plotted in Figs. 10 and 11, respectively. In all cases, it can be seen that the apparent shear stress (thus pressure) oscillates between the same two extreme values irrespective of the rate. In addition, the frequency of these oscillations increases with increasing shear rate and the amount of material in the reservoir of the capillary rheometer. The explanation for the periodicity of these pressure oscillations is given in terms of a very simple mathematical model that includes the compressibility and slip of polyethylenes as essential ingredients in obtaining such behavior (Hatzikiriakos and Dealy 1992b).

Table 1 summarizes the critical shear rates for the onset of sharkskin, stick-slip and gross melt fracture where applicable. It can be seen that the EF606 LDPE exhibits the onset of gross melt fracture at a relatively low apparent shear rate of 50 $s^{-1}$, followed by the other LDPE (LD200) that fractures at a rate of 270 $s^{-1}$. Despite exhibiting flow curve discontinuities and sharkskin at low apparent shear rates, the onset of gross melt fracture for the two LLDPEs does not occur until higher shear rates, specifically at 420 $s^{-1}$ for the Exact 3128 polymer and at a rate of 1400 $s^{-1}$ for the LL3001.32.

## Peeling experiments

As discussed above peel specimens consisting of thin polymer strips confined between paper substrates were subjected to peeling at an angle of 180° (t-peel geometry) using various peeling rates at a melt temperature of 150 °C. Figure 12 contains typical transient peeling results for the Exact 3128 polymer for a variety peel rates depicted in terms of the peel strength that is the peeling force normalized by the width of the strip as a function of the peel length that is the length of polymer peeled from the paper. At low peeling rates the force increases and attains a steady-state value as indicated by the transient peel strength data at a peeling rate of 0.33 cm/s. The type of failure observed at these low rates of peel is purely cohesive in nature as polymer remains present on the peeled paper substrates. In this cohesive peel failure regime, the steady-state peel strength increases monotonically with peel rate. However, at a critical rate the peel strength signal becomes unstable over the duration of the peeling test manifested by the periodic oscillation of the transient response between maximum

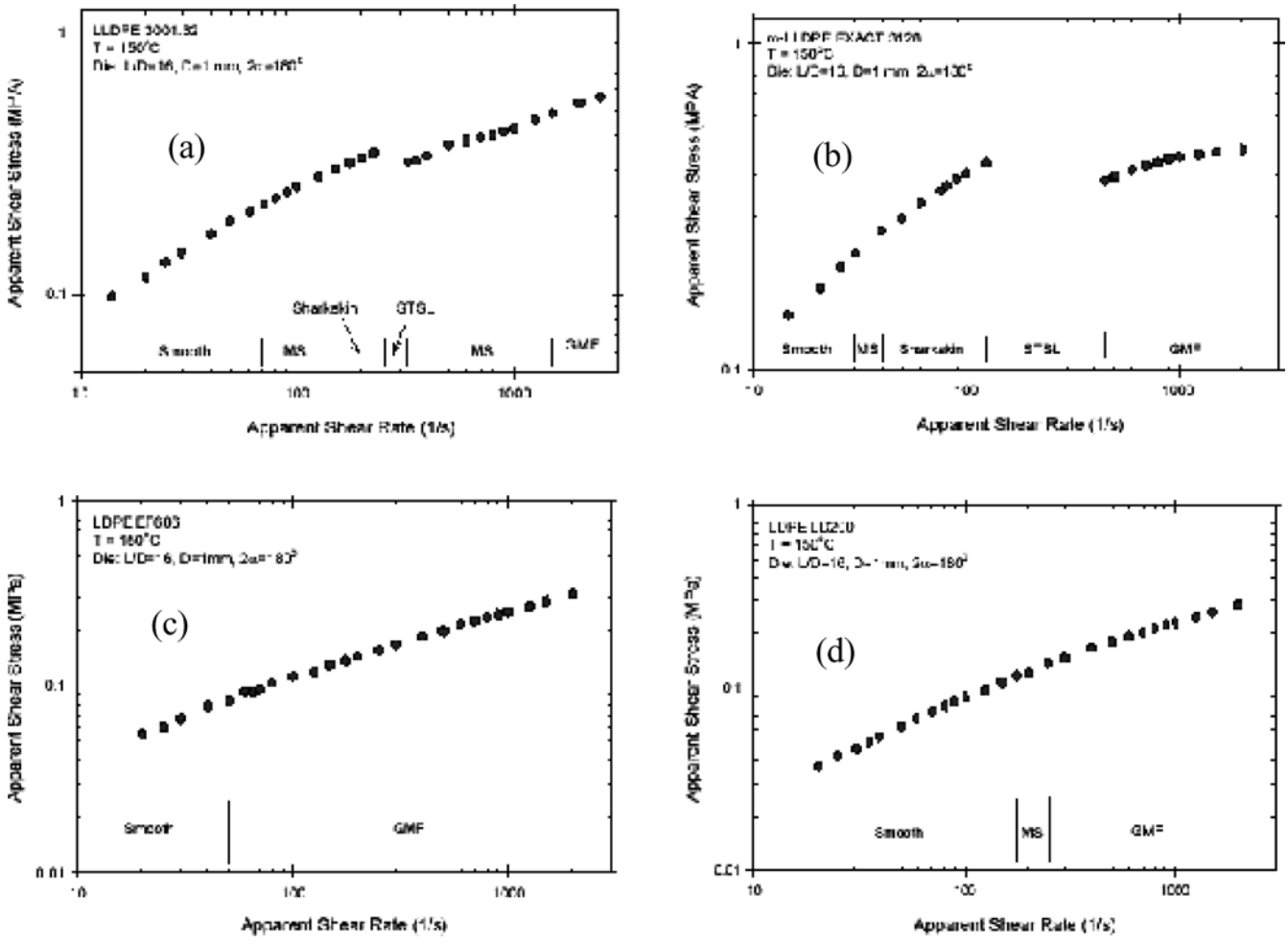


**Fig. 7a–d** The apparent flow curves at a melt temperature of 150 °C obtained from a capillary rheometer using a capillary having L/D = 16, D = 1 mm and a contraction angle of 180° for: **a** LL3001.32; **b** Exact 3128; **c** EF606; **d** LD200. Key to text captions designating extrudate appearance: Smooth—smooth extrudate surface, MS—minor scratches, Sharkskin—sharkskin melt fracture, STSL—oscillating/stick-slip flow regime, GMF—gross melt fracture

and minimum peel strength values. The type of peel failure under these circumstances is stick-slip in nature as traces of polymer remain on the paper in a periodic fashion corresponding to the transient peel strength signal. During the transient peel strength rise the peel failure is cohesive with the molten polymer remaining on the paper, whereas during the transient decay portion of the signal the failure becomes adhesive. Hence, as the peel strength assumes a critical value the interface fails adhesively manifested by the delamination of the molten polymer from the paper substrate. Figure 13 contains a plot of a transient stick-slip experiment with the Exact 3128 melt at a peel rate of 0.7 cm/s superposed with a picture of the peeled specimen for that experiment. Remnants of the polymer and the mating surface peaks are clearly evident on the portions of the paper substrate corresponding to the cohesive failure-related peel strength rises of the transient signal. Likewise, delamination is clearly evident on the portions of the paper substrate corresponding to the adhesive failure peel strength decay of the transient signal. At higher peeling rates, the peel strength signal exhibits a maximum followed by a rapid decay to a steady-state as shown for the data at peeling rates of 3.333 cm/s and 10 cm/s. Under these circumstances the peel failure is always adhesive manifested by a complete interfacial delamination of the polymer melt from one of the peel specimen substrates.

Figure 14 contains plots of typical peel strength transients for a LDPE (EF606) that exhibit a striking difference in behavior from the LLDPE. Unlike the LLDPE, stick-slip behavior is never observed with the LDPE melt and the peel strength traces always result in steady-state values that increase with peel rate. At low rates of peel the failure is cohesive; however at a critical rate of peel the type of failure observed becomes semicohesive in nature manifested by a multi-dendritic


**Fig. 8** Typical extrudate photos of LLDPE (LL3001.32) at 150 °C obtained from a capillary rheometer using a capillary having L/D = 16, D = 1 mm and a contraction angle of 180 °C

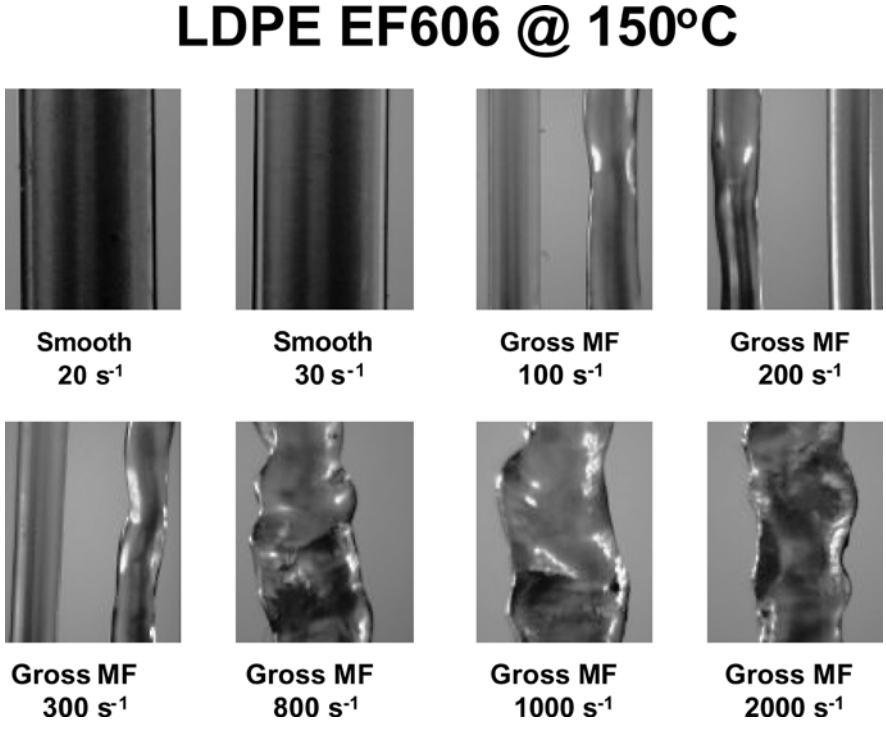


**Fig. 9** Typical extrudate photos of LDPE (EF606) at 150 °C obtained from a capillary rheometer using a capillary having L/D = 16, D = 1 mm and a contraction angle of 180°

failure surface. In other words, porous looking thin films of the polymer appear on the peel specimen substrate akin to an adhesive/cohesive-type of failure phenomenon. At still higher rates of peel, the failure becomes purely adhesive but unlike its linear counterpart the observance of complete interfacial delamination is not accompanied by a decrease in peel strength.

Figure 15a,b summarizes the peeling test results in terms of peel strength versus peel rate for the LLDPEs and LDPEs, respectively. With increasing rate of peel

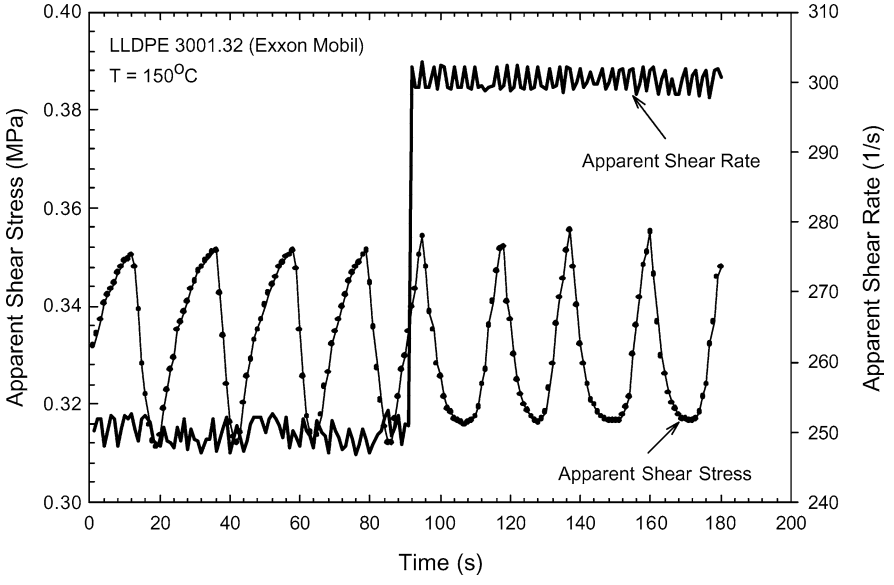


**Fig. 10** Stick-slip transients obtained for LL3001.32 in the capillary rheome ter at 150 °C

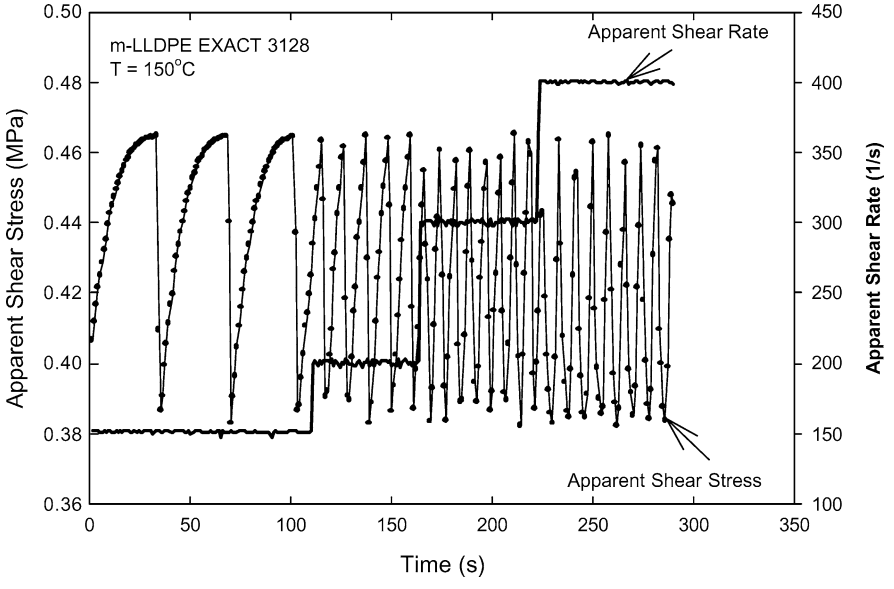


**Fig. 11** Stick-slip transients obtained for Exact 3128 in the capillary rheometer at 150 °C

with the LLDPEs (Fig. 15a), cohesive failure (steady peeling) is replaced by an unstable stick-slip regime that periodically oscillates between cohesive and adhesive modes of failure (unsteady peeling) characterized by maximum and minimum values in peel strength, which in turn is replaced by a purely adhesive mode of failure (steady peeling). It should be noted that the Exact 3128 polymer exhibits a broader region of peel instability than the LL3001.32, an observation that will be revisited shortly. In addition, following the peel instability regime both LLDPEs exhibit a broad range of peel rates in which the peel strength remains semi-constant before monotonically increasing with rate once again. Figure 15b shows the results for the LDPEs where although the mode of peeling failure exhibits a transition at a critical rate the peeling behavior is never unstable. Note as well that the film grade LLDPEs and LDPE eventually exhibit purely adhesive failure (complete interfacial delamination) at high enough peel rates; however, the coating grade LDPE never exhibits such adhesive failure up to a peeling rate of 200 cm/s. This observation pro-

**Table 1** Critical apparent shear rates ($s^{-1}$) for the onset of instabilities at 150 °C

| Polymer | Sharkskin MF | Stick-slip | Gross MF |
|---|---|---|---|
| LLDPE Exact 3128 | 20 | 120 | 420 |
| LLDPE LL3001.32 | 70 | 240 | 1400 |
| LDPE LD200 | - | - | 270 |
| LDPE EF606 | - | - | 50 |

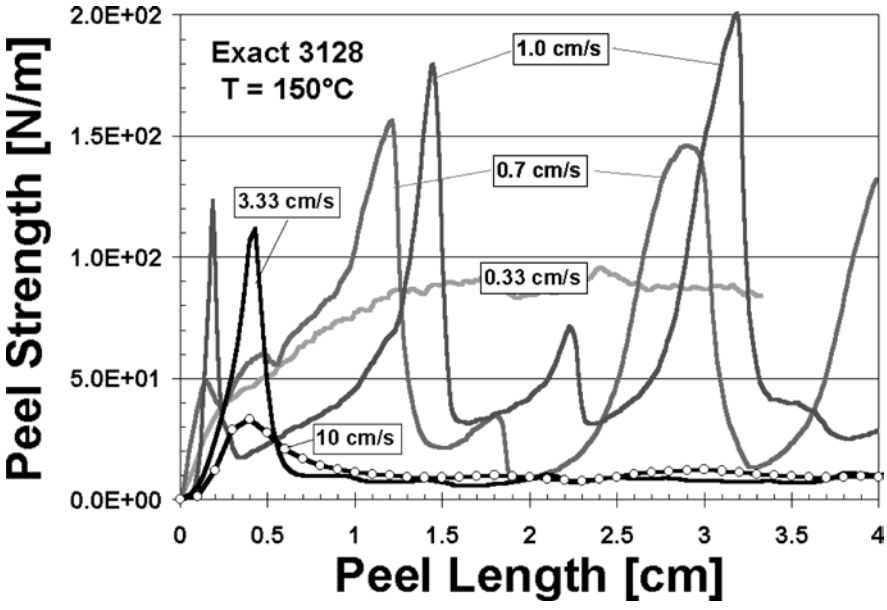


**Fig. 12** Transient peel strength traces for peel experiments with Exact 3128 at a melt temperature of 150 °C and various peeling rates

vides a direct illustration as to the desired behavior of a polymer utilized for coating application, in which interfacial delamination is inherently unacceptable.

## Discussion and conclusions

The experimental results presented herein elucidate certain rheological melt flow characteristics that provide fundamental insight into melt processing behavior. In particular, high-rate extensional melt flow behavior appears to play a critical role in observed melt flow phenomena such as sharkskin, oscillating flow, and gross melt fracture. As described earlier, the onset of sharkskin is believed to be due to a localized melt rupture phenomenon initiated at the free surface of the extrudate and propagated inward upon exiting the die. The singularity that occurs at the die exit as the melt abruptly transitions from a fixed boundary to a free surface results in high extensional flow deformations isolated to the region of the melt nearest the "skin" of the extrudate. The periodicity of the sharkskin melt fracture comes as a result of the intermittent elastic energy storage via tensile modulus increase and elastic energy

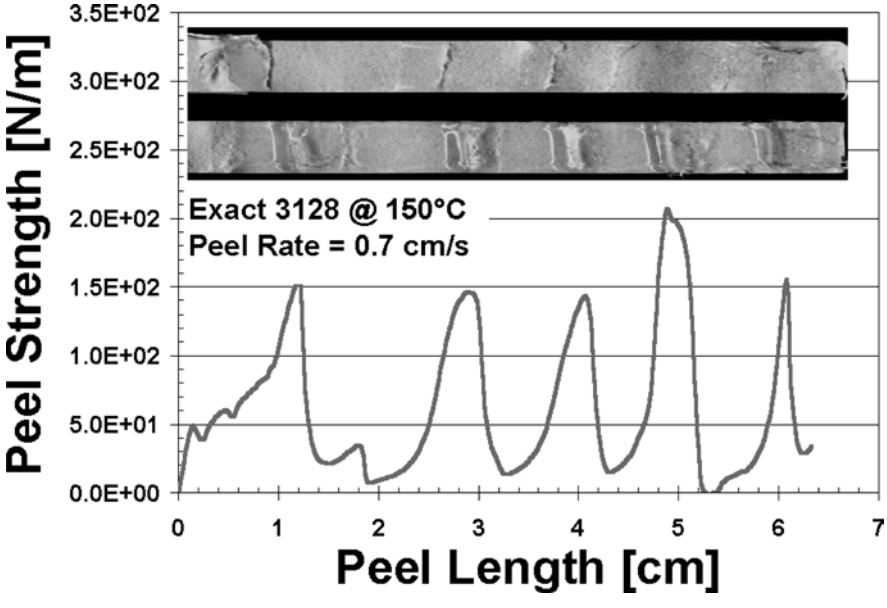


**Fig. 13** A transient peeling experiment indicating stick-slip along with a photo showing the cohesive failure during the ascending part of the peel strength and the adhesive failure during the descending part of the peel strength

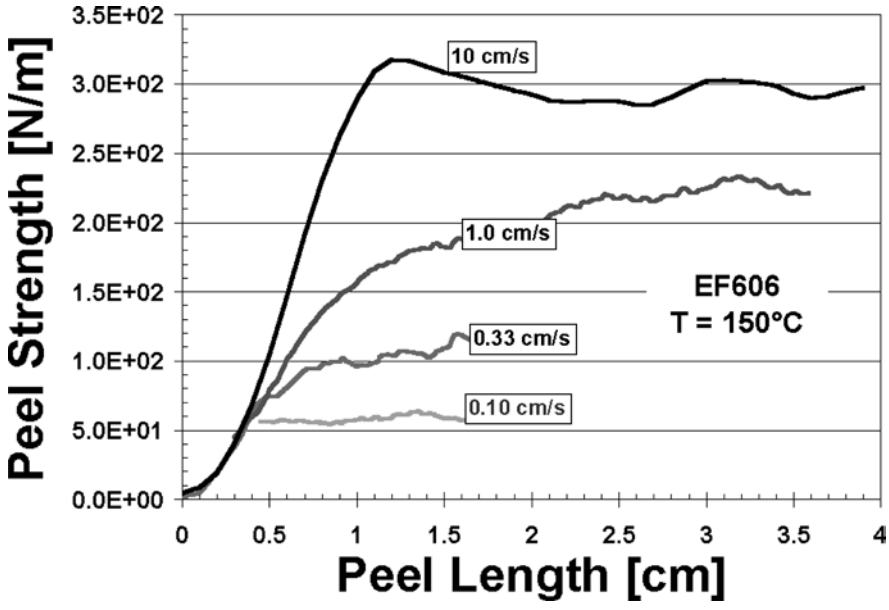


**Fig. 14** Transient peel strength traces for peel experiments with EF606 at a melt temperature of 150 °C and various peeling rates

dissipation via transverse crack propagation along the surface region of the extrudate. Consequently, linear polyethylenes are prone to this type of sharkskin melt fracture phenomenon due to the fact that at high extensional flow rates they exhibit both a rapid increase in elastic tensile modulus and a brittle-type mode of failure at rupture, factors that inherently contribute to crack propagation. Because of the tensile retardation mechanism described earlier, branched polymer extrudates are inherently resistant to such type of melt rupture upon exiting the die. The impact of high-rate tensile retardation on melt fracture phenomena was recently investigated by Sentmanat and Hatzikiriakos (2004) who demonstrated that the presence of a minute amount (0.1%) of an adsorptive boron nitride filler acts as an energy dissipater that reduces the elastic tensile modulus of linear low density polyethylenes at high extensional flow rates. In addition, their capillary extrusion experiments revealed that the presence of the filler eliminated sharkskin and delayed the onset of gross melt fracture. They concluded that since exit flow is a stress-governed event, the dissipative energy effects of the Boron Nitride served to ''plasticize'' the regions of the polymer extrudate undergoing high extensional flow deformation thereby eliminating the localized surface melt rupture that otherwise might have occurred. Other investigators (Achilleos et al.2002) have noted the importance of decreasing the magnitude of extensional flow at the die exit through the use of low surface energy, slip promoting fluoropolymer coatings near the exit region of the capillary resulting in the elimination of sharkskin.

Comparing the peel results from Fig. 15a,b with the corresponding flow curves of these polymers in extrusion (Fig. 7a–d), we can easily identify similarities. In particular, the peel curves for the LLDPEs in Fig. 15a exhibit the same general characteristics exhibited by the flow curves of Fig. 7a,b. Not only do the peel curves exhibit a similar region of instability exhibited only by the linear polymers, the region of peel instability is broader with the Exact 3128 polymer as is the oscillating flow regime of the apparent flow curve for Exact 3128. Furthermore, these experimental results provide compelling evidence that the flow in this extrusion regime is indeed stick-slip in nature manifested by the intermittent transition between a no-slip boundary condition and adhesive failure at the die wall. In addition, the melt flow instabilities in peel and extrusion are believed to come as a result of the rapid increase in elastic tensile modulus at high rates of deformation observed with the LLDPEs. Although peel flow is by no means simple, the large deformations generated in the advancing peel melt fracture front bear many of the traits of uniaxial extension (albeit non-uniform) particularly for large peel rates. With any peel deformation there is a delicate balance between the deforming melt's cohesive strength and its adhesive strength at the substrate interface. As the peel rate of the LLDPEs increases, the rapid increase in elastic tensile modulus causes an increase in cohesive melt strength, which at a critical stress initiates an adhesive failure at the substrate interface. If the polymer melt still in the nip region of the peel front has sufficient time to relax from this induced strain hardening then the interfacial stress falls below the critical adhesive limit resulting in a rapid transition to cohesive peel failure. In this manner, the nonlinear viscoelastic extensional flow properties of the polymer melt dictate the dynamics of peel behavior resulting in intermittent cohesive and adhesive failure as exhibited by the unstable peel frac-

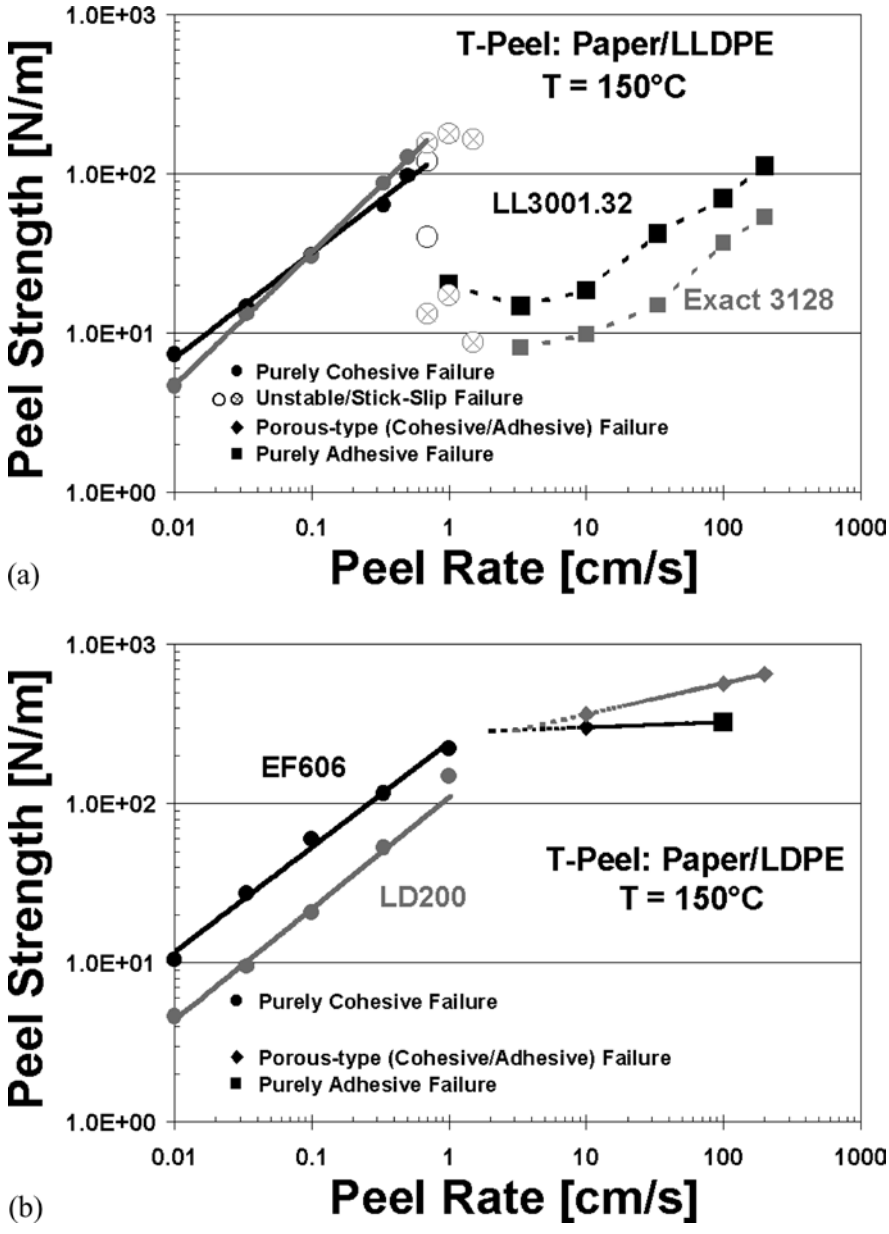


**Fig. 15a,b** The peel strength curves as a function of peel rate at a melt temperature of 150 °C for: **a** the LLDPEs LL3001.32 and Exact 3128; **b** the LDPEs EF606 and LD200

ture specimen in Fig. 13. At rates above this regime of peel behavior, the polymer melt in the nip region no longer has time to relax from the induced strain hardening, and hence the peel fracture transitions from an unstable stick-slip to a purely adhesive mode of failure. Similarly, it is argued that the LLDPEs in the oscillating flow regime of extrusion exhibit intermittent stick-slip in the die land region and that the rate-dependent breadth of this stick-slip instability is a function of the rapidity in elastic tensile modulus growth at high rates of deformation. Recalling Figs. 6, 7c,d and 15b, the fact that the LDPEs exhibit no such type of flow instability either in peel or extrusion appears to support this assertion with regard to rapid tensile stress growth behavior.

Observations with regard to the onset of gross melt fracture for all of the polymers can be correlated with the extensional viscosity curves of Fig. 16 that were taken from the peaks of the tensile stress growth plots of Fig. 5a,b. Note how the critical shear rates for the onset of gross melt fracture from Table 1 are inversely correlated with the extensional viscosity behaviors depicted in Fig. 16 for elevated Hencky strain rates. This trend is consistent with prior literature that has reported that gross melt fracture originates at the entrance to the capillary and is due to a critical extensional stress value (Cogswell1972, 1977a, 1977b; Kim and Dealy 2002a, 2002b).

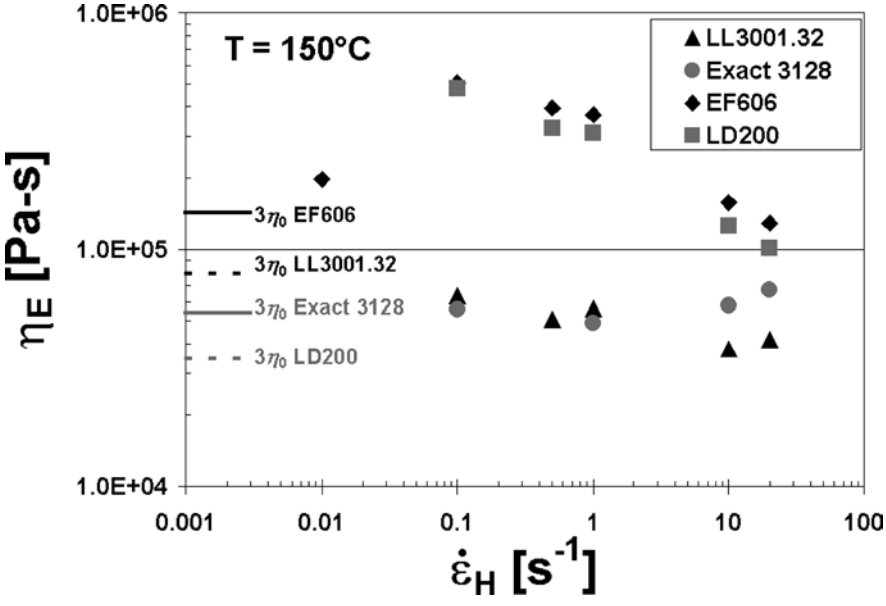


**Fig. 16** Comparison of the steady extensional viscosity as a function of Hencky strain rate for all four polymers at a melt temperature of 150 °C

Based on these experimental observations, extensional melt flow experiments together with melt peel experiments provide first a fingerprint of the flow curve of polyethylenes and second valuable insight into fundamental melt polymer processing behavior particularly with regard to the sharkskin melt fracture, oscillating flow, and gross melt fracture behaviors inherent with the extrusion of polyethylene.

**Acknowledgements** This work was financially supported by a strategic grant provided by NSERC Canada.

## References


Achilleos EC, Georgiou G, Hatzikiriakos SG (2002) The role of processing aids in the extrusion of molten polymers. J Vinyl Additive Technol 8:7–24

Anastasiadis SH, Hatzikiriakos SG (1998) The work of adhesion of polymer/wall interfaces and its association with the onset of slip. J Rheol 42:795–812

Bagley EB, Cabott IM, West DC (1958) Discontinuity in the flow curve of polyethylene. J Appl Phys 29:109–110

Blyler LL, Hart AC (1970) Capillary flow instability of ethylene polymer melts. Polym Eng Sci 10:193–203

Cogswell FN (1972) Converging flow of polymer melt in extrusion dies. Polym Eng Sci 12:64–73

Cogswell FN (1977a) Streching flow instabilities at the exits of extrusion dies. J Non-Newtonian Fluid Mech 2:37–47

Cogswell FN (1977b) Converging flow and stretching flow: a compilation. J Non-Newtonian Fluid Mech 4:23–38

El-Kissi N, Piau JM (1994) Adhesion of linear low-density polyethylene for flow regimes with sharkskin. J Rheol 38:1447–1463

Hatzikiriakos SG (1993) A slip model for linear polymers based on adhesive failure. Int Polym Process 8:135–142

Hatzikiriakos SG, Dealy JM (1992a) Wall slip of molten high density polyethylenes. II. Capillary rheometer studies. J Rheol 36:703–741

Hatzikiriakos SG, Dealy JM (1992b) Role of slip and fracture in the oscillating flow of HDPE in a capillary. J Rheol 36:845–884

Hill DA, Hasegawa T, Denn MM (1990) On the apparent relation between adhesive failure and melt fracture. J Rheol 34:891–918

Inn YW, Wang LS, Shaw MT (2000) Efforts to find stick-slip flow in the land of a die under sharkskin melt fracture conditions: polybutadiene. Macromol Symp 158:65–75

Kalika DS, Denn MM (1987) Wall slip and extrudate distortion in linear low-density polyethylene. J Rheol 31:815–834

Kim S, Dealy JM (2002a) Gross melt fracture of polyethylene. I. A criterion based on tensile stress. Polym Eng Sci 42:482–494

Kim S, Dealy JM (2002b) Gross melt fracture of polyethylene. II. Effects of molecular structure. Polym Eng Sci 42:485–503

Legrand F, Piau JM (1998) Spatially resolved stress birefringence and flow visualization in the flow instabilities of a polydimethylsiloxane extruded through a slit die. J Non-Newtonian Fluid Mech 77:123–150

Lupton LM, Regester JW (1965) Melt flow of polyethylene at high rates. Polym Eng Sci 5:235–245

McLeish TCB, Larson RG (1998) Molecular constitutive equations for a class of branched polymers: the Pom-Pom model. J Rheol 42(1):81–110

Migler KB, Lavallée C, Dillon MP (2001) Visualizing the elimination of sharkskin through fluoropolymer additives: coating and polymer-polymer slippage. J Rheol 45:565–581

Myerholtz RW (1967) Oscillating flow behavior of high-density polyethylene melts. J Appl Polym Sci 11:687–698

Ramamurthy AV (1986) Wall slip in viscous fluids and influence of materials of construction. J Rheol 30:337–357

Sentmanat ML (2003a) A novel device for characterizing polymer flows in uniaxial extension. ANTEC '03, Soc Plastics Eng'rs, Tech. Papers, 49, CD-ROM, New York

Sentmanat ML (2003b) Dual windup extensional rheometer. US Patent 6,578,413

Sentmanat ML (2004) Miniature Testing Platform: from extensional melt rheology to solid state deformation behavior. Rheol Acta (accepted)

Sentmanat ML, SG Hatzikiriakos (2004) Mechanism of gross melt fracture elimination in the extrusion of polyethylenes in the presence of boron nitride. Rheol Acta (in press)

Sentmanat ML, Wang B, McKinley GH (2004) Measuring the transient extensional rheology of a LDPE melt using the SER Universal Testing Platform. J Rheol (submitted)

Smoluk GR (1964) Velocity profiles for polyethylene melts. Plast Eng 115–131

Wang SQ, Drda PA, Inn YW (1996) Exploring molecular origins of sharkskin, partial slip, and slope change in flow curves of linear low density polyethylene. J Rheol 40:875–898